NUMERICAL STUDY OF HEAT AND MASS TRANSFER ENHANCEMENT FOR BUBBLE ABSORPTION PROCESS OF AMMONIA-WATER MIXTURE WITHOUT AND WITH NANOFLUIDS

by

Mohamed Bechir BEN HAMIDA*, Jalel BELGHAIEB, and Nejib HAJJI

Research Unit of Energy and Environment, National School of Engineers of Gabes, University of Gabes, Gabes, Tunisia

Original scientific paper
https://doi.org/10.2298/TSCI170313229B

This paper presents a detailed analysis of a combined heat and mass transfer enhancement by using binary nanofluid in NH_3/H_2O bubble absorption processes. A differential mathematical model of ammonia-water absorption has been developed on the basis of mass and energy balances and heat and mass transfer equations, in order to analyses the effects of binary nanofluid on ammonia absorption. A finite difference technique was employed to solve the numerical model. A parametric analysis was conducted to assess the effect of key parameters: the effective absorption rate, the concentration of nanoparticles, kinds of additives of nanoparticles, the bubble diameter, and the gas holdup on the performance of the absorber. As expected, the addition of nanoparticles enhances the absorption performance during the bubble absorption process. Also, it is found that the highest effective absorption ratio was reported for solution with copper. The concentration of nanoparticles has a significant effect on the absorber size.

Key words: *nanofluid, ammonia-water, bubble absorption, mass transfer, heat transfer*

Introduction

There are several refrigeration systems based on the absorption phenomenon that are used in many applications such as automobiles [1], solar water distillation [2], *etc.* They use as pairs of fluid ammonia-water [3, 4], LiBr-water and CO_2-water [5]. In order to increase the performance of these systems, one of the solutions is to use the nanofluid which enhance the heat and mass transfer processes of absorption refrigeration system. Recently, nanofluids have been an active field of research due to its greatly enhanced thermal properties [6]. Binary nanofluid as the nanofluid in which the base fluid is a binary mixture such as ammonia-water, a definition reported by Kim *et al.* [7]. The effect of mono Ag nanoparticles on heat and mass transfer characteristics in NH_3/H_2O bubble absorption process were studied by Wu *et al.* [8]. Their result found that the effective absorption ratio can reach the maximum of 1.55 when the mono Ag concentration is 0.02% and the initial ammonia concentration is 20%. Pang *et al.* [9] have experimentally investigated the heat and mass transfer enhancement by using binary nanofluid in the bubble type absorber. Mono Ag are used to produce the binary nanofluids (NH_3/H_2O binary mixture with Ag nanoparticles). The ammonia-water bubble absorption ex-

* Corresponding author, e-mail: benhamida_mbechir@yahoo.fr

periments are carried out under the condition with/without the coolant (water). Their result found that the mass transfer in binary nanofluids with the coolant is enhanced more than that without the coolant. Also, result show that the absorption rate with 0.02% Ag nanoparticles is enhanced as high as 55% compared to the base fluid. Enhancement in absorption with carbon nanotubes (CNT) was studied by Ma *et al.* [10]. The CNT had a weight percentage of 0-0.5 percent, a length of 5-10 μm and diameter of 20 nm. Their results show that the absorption rates of the CNT-ammonia binary nanofluids are higher than those of ammonia solution without CNT. Also, result found that the effective absorption ratio of the CNT-ammonia binary nanofluids increase with the initial ammonia concentration. The CNT-ammonia binary nanofluids have remarkable higher effective thermal conductivity ratio than the base fluids. The concentration of ammonia has an insignificant influence on the effective thermal conductivity ratio of the binary nanofluid. Other researchers have studied the enhancement of water-lithium bromure falling film absorption process with the use of binary nanofluids with Fe nanoparticles and CNT. Results found that the vapor absorption rate increases with increasing the concentration of CNT and Fe nanoparticles and the solution mass flow rate. It has been show that the mass transfer enhancements is much more significant than heat transfer in the binary nanofluids with CNT and Fe. The mass transfer enhancement from the Fe nanoparticles becomes lower than that from the CNT nanoparticles. Su *et al.* [12] developed a numerical model for ammonia absorption from a bubble expanding at a submerged nozzle into a binary nanofluid. The effects of the flow rate of ammonia vapor, the radius of nozzle and the concentration of nanoparticles on mean absorption rate were studied. Their result found that the flow rate of ammonia vapor and the diameter of the nozzle hardly affect the enhancement of the binary nanofluid for the absorption of bubble growing stage. The enhancement of binary nanofluid for bubble absorption has the analogous tendency with the mass transfer enhancement of binary nanofluid. Yang *et al.* [13] have experimentally studied the enhancement of ammonia-water falling film absorption by adding nanoparticles. The effect of addition three nanoparticles: Fe_2O_3, Al_2O_3, and $ZnFe_2O_4$, and surfactant sodium dodecyl benzene sulfonate (SDBS) was measured. A vertical tubular absorber of 25 mm diameter with coupling fluid circulated on the inside of the tube, and solution flowing as a falling film on the outside of the tube was considered. Results reveal that addition of nanoparticles increases the absorption rate by introducing micro-convection and enhancing the effective thermal conductivity. The effective absorption ratio can be increased by 50% with $ZnFe_2O_4$ nanofluid and by 70% with Fe_2O_3 nanofluid for 15% ammonia-water solution. The enhancement was found to be higher for nanofluids made from Fe_2O_3. Other experimental studies investigated the enhancement of ammonia-water bubble absorption with the use of nanoparticles Kim *et al.* [14]. The effect of three types of nanoparticles namely Cu, CuO, and Al_2O_3 and their concentration on the absorption performance was examined. Results showed that presence of nanoparticles in the solution enhanced the absorption process. They also defined the effective absorption ratio which was the absorption rate of the binary nanofluids divided by the absorption rate of binary base fluids. Increasing the solution concentration increase the effective absorption ratio. The highest effective absorption ratio was reported for solution with Cu. Lee *et al.* [15] have experimentally investigated the effect of nanoparticles on the absorption heat transfer enhancement. The CNT and Al_2O_3 nanoparticles are added to prepare the binary nanofluids in the binary mixture of NH_3/H_2O. Their results show that absorption rate and heat transfer rate with 0.02% CNT nanoparticles become 17% and 16 % higher than those without nanoparticles. Also, result found that nanofluids made from Al_2O_3 exhibited the highest increase in absorption rate among the CNT particles. Many studies focused on falling film absorption with nanofluids

have been performed. Kim *et al.* [16] conducted an experimental study of enhancement of water-lithium bromure falling film absorption by adding SiO_2 nanoparticles. The effect of the concentration of SiO_2 nanoparticles and the base fluid concentration was examined. Results revealed that the enhancement ratios in the heat and mass transfer were found to be higher for 0.005% SiO_2 nanoparticles concentration (an enhancement of nearly 46.8% and 18% for heat and mass transfer rates respectively).

The objective of this paper is to investigate the combined heat and mass transfer enhancement using binary nanofluids for bubble absorption process and to find the effect of some parameters such as the concentration of nanoparticles, kinds of additives of nanoparticles, the diameter of orifice, the number of orifice and the inlet solution temperature on the performance of the absorber. A numerical model of ammonia bubble absorption with the use of nanoparticles was established by considering the variation in physical proprieties of the mixture when adding nanoparticles.

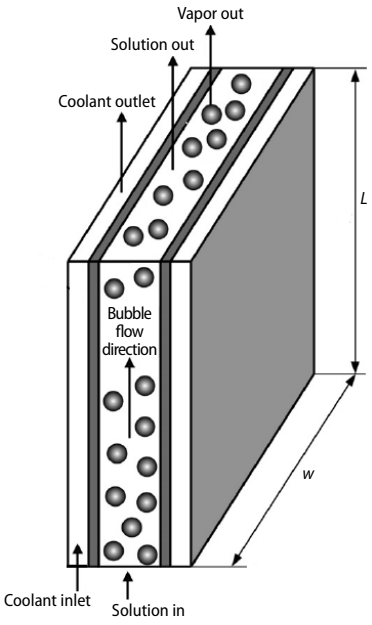

Figure 1. Schematic diagram of the plate type bubble absorber

Problem formulation

Position of the problem

A schematic illustration of the vertical tubular absorber is shown in fig. 1.

The absorber consists of two types of canal, that is, the absorption canal and the cooling canal. In the absorption canal, the ammonia vapor and the weak ammonia-water liquid solution are distributed at the bottom of the absorber and circulate co-currently. The vapor enters at the bottom of the absorber and is distributed into the canal through small diameter orifice. The weak solution is also introduced at the bottom of the absorber, going into the canal through the free area between canal and orifice. The absorption process progresses as the vapor and weak solution contact inside the tubes. The cooling water flows in the same direction as that of the vapor but in the cooling canal.

The operational conditions and geometric considered in this paper are summarized in tabs. 1 and 2.

Hypotheses

For mathematical formulation of the problem, which describes the heat and mass transfer processes, the following assumptions are made during the model development.

– The nanofluids cannot be compressed.
– Absorption process is assumed to be in steady-state.
– System pressure is constant.
– Thermodynamic equilibrium exists at the liquid-vapor interface.
– No direct heat transfer between the vapor and the coolant.
– Bubble break-up and coalescence not considered.
– The bubble is assumed to be spherical.

Table 1. Operating conditions of the co-current absorber

System pressure, [bar]	2.87
Coolant medium	Water
Inlet conditions	
Solution mass flow rate, [kgs^{-1}]	0.097
Solution bulk temperature, [K]	297.03
Solution mass fraction [kgkg^{-1}]	0.4496
Nanoparticle	
Kinds Copper (Cu)	
Copper oxide (CuO)	
Aluminum oxide (Al_2O_3)	
Mass fraction of nanoparticles, [%]	0-0.2
Vapor mass flow rate, [kgs^{-1}]	0.042919
Vapor bulk temperature, [K]	302.59
Vapor mass fraction, [kgkg^{-1}]	0.9999
Coolant bulk temperature, [K]	302.59
Coolant mass flow rate, [kgs^{-1}]	2.46

Table 2. Geometric dimensions of the co-current absorber

Diameter of orifice, [m]	0.085
Number of orifice	750
Area of orifice, [m^2]	$5.67 \cdot 10^{-3}$
Cooling plate length, L, [m]	1.7
Thermal conductivity, [Wm^{-1}K^{-1}]	13
Thickness of the cooling plates, [m]	0.002

Mass transfer equations

In the considered system, the mass transfer between the vapor and the liquid phases is due to the combined contribution of bulk transport and molecular diffusion of ammonia and water across the interface. The total molar flux absorbed/desorbed is the sum of ammonia N_{NH_3} and water N_{H_2O} molar fluxes, can be given by eq. (1):

$$N_{NH_3} + N_{H_2O} = K_L R_{eff} \ln\left(\frac{z - x_L}{z - x_{Li}}\right) = K_v R_{eff} \ln\left(\frac{z - x_{vi}}{z - x_v}\right) \tag{1}$$

where the subscripts L, v, and i stand for liquid, vapor, and liquid-vapor interface, respectively, and z is defined as the ratio of the ammonia molar flux absorbed/desorbed to the total molar flux absorbed/desorbed.

In order to carry out the mass continuity requirement at the interface, the mass transport from the vapor should be equal to the bulk liquid, as expressed in eq. (2):

$$N_{NH_3} = N_{H_2O} \tag{2}$$

The R_{eff} is the effective absorption ratio is defined as the ratio of the absorption rate in the case with addition of nanoparticles to that in the case without any addition.

$$R_{eff} = \frac{\dot{m}_{abs,\ binary\ nanofluid}}{\dot{m}_{abs,\ base\ fluid}} \tag{3}$$

Therefore, the physical meaning of the effective absorption ratio is the effectiveness of the addition for absorption enhancement. That is if R_{eff} is larger than 1, the addition enhances the absorption performance. If R_{eff} less than 1, it can be said that the addition has the negative effect to the absorption performance.

In this work, the experimental correlations of the effective absorption ratio R_{eff} are developed with respect to the initial concentration of nanoparticles and ammonia in binary nanofluid. Because the effective absorption ratio R_{eff} is linearly proportional to concentration of nanoparticles and second orderly proportional to ammonia concentration, Kim *et al.* [14]:

$$R_{eff} = (c_0 + c_1 x_{NH_3} + c_2 x_{NH_3}^2) + (d_0 + d_1 x_{NH_3} + d_2 x_{NH_3}^2)\, phi \tag{4}$$

where the coefficients of the experimental correlations for all nanoparticle used is shown in tab. 3.

Heat and mass transfer coefficients

In the present model, the liquid-side mass transfer coefficient is obtained by the correlation proposed by Akita and Yoshida [17]:

$$K_{\mathrm{L}}=\frac{0.5\beta_{\mathrm{L}}}{d_{\mathrm{B}}}\left(\frac{\mu_{\mathrm{L}}}{\rho_{\mathrm{L}}\beta_{\mathrm{L}}}\right)^{0.5}\left(\frac{\mathrm{g}d_{\mathrm{B}}^{3}\rho_{\mathrm{L}}^{2}}{\mu_{\mathrm{L}}^{2}}\right)^{0.25}\left(\frac{gd_{\mathrm{B}}^{2}\rho_{\mathrm{L}}}{\sigma}\right)^{3/8} \quad (5)$$

where d_{B}, β_{L}, ρ_{L}, μ_{L}, and σ are diameter of bubble, diffusivity of liquid phase, density of liquid phase, viscosity of liquid phase, and surface tension, respectively.

Table 3. The coefficients of the experimental correlations for all nanoparticle

Coefficients	Copper	Copper oxide	Aluminum oxide
c_0	1.125	1.072	1.067
c_1	–0.035	0.014	0.018
c_2	0.005	0.002	0.001
d_0	9.092	8.248	8.552
d_1	0.433	–0.048	–0.196
d_2	–0.023	0.01	0.016

The vapor-side mass transfer coefficient was calculated using a correlation obtained from Clift *et al.* [18]:

$$K_{\mathrm{v}}=1.4\frac{AC_{p_{\mathrm{v}}}}{A_{\mathrm{p}}}\left(\frac{\mathrm{Sc}_{\mathrm{v}}}{\mathrm{Pr}_{\mathrm{v}}}\right)^{2/3}\left[\frac{48\sigma\beta_{\mathrm{v}}^{2}}{\pi^{2}d_{\mathrm{B}}\rho_{\mathrm{L}}\left(2+3\dfrac{\rho_{\mathrm{v}}}{\rho_{\mathrm{L}}}\right)}\right]^{1/4} \quad (6)$$

where A, A_{p}, $C_{p_{\mathrm{v}}}$, β_{v}, Sc_{v}, and Pr_{v} are area, projected area, specific heat of vapor, diffusivity of vapor, Schmidt number, and Prandtl number, respectively.

The convective heat transfer coefficient between the weak solution and the interface, h_{L} is obtained using the Chilton and Colburn [19] analogy, which provides a relationship between heat and mass transfer coefficients, according to eq.(5).

$$h_{\mathrm{L}}=C_{p_{L}}K_{\mathrm{L}}\left(\frac{\mathrm{Sc}_{\mathrm{L}}}{\mathrm{Pr}_{\mathrm{L}}}\right)^{2/3} \quad (7)$$

Similarly, the convective heat transfer coefficient between the vapor and the interface, h_{v}, was calculated using a correlation obtained from Chilton and Colburn [19]:

$$h_{\mathrm{v}}=C_{p_{\mathrm{v}}}K_{\mathrm{v}}\left(\frac{\mathrm{Sc}_{\mathrm{v}}}{\mathrm{Pr}_{\mathrm{v}}}\right)^{2/3} \quad (8)$$

where Schmidt number and Prandtl number are defined:

$$\mathrm{Sc}=\frac{\mu}{\rho D} \quad (9)$$

$$\mathrm{Pr}=\frac{\mu C_{p}}{k} \quad (10)$$

Heat transfer equations

In general, heat transfer between the vapor and the liquid phase due to convection occurs due to temperature gradient between two surfaces. However the heat transfer occurs not only due to convection but also due to the sensible heat load. If this heat transfer is also accompanied by mass transfer across the bounding surface, then an additional amount of heat will be

added due to the heat capacity of the mass. Hence the convective heat transfer coefficient h can be modified to account for the effect of mass transfer. The modified heat transfer coefficient h^* is given by Treybal [20]:

$$h^* = h\frac{c}{1-\exp(-c)} \tag{11}$$

with c being:

$$c = \frac{N_{\mathrm{NH_3}} C_{p_{\mathrm{NH_3}}} + N_{\mathrm{H_2O}} C_{p_{\mathrm{H_2O}}}}{h} \tag{12}$$

The sensible heat of the liquid transferred to the interface is given by equation:

$$Q_{\mathrm{senL}} = h_{\mathrm{L}}^* \mathrm{d}A(T_{\mathrm{i}} - T_{\mathrm{L}}) \tag{13}$$

$$c_{\mathrm{L}} = \frac{N_{\mathrm{NH_3}} C_{p_{\mathrm{NH_3L}}} + N_{\mathrm{H_2O}} C_{p_{\mathrm{H_2OL}}}}{h_{\mathrm{L}}} \tag{14}$$

The sensible heat of the vapor that is transferred to the interface is given:

$$Q_{\mathrm{senv}} = h_{\mathrm{v}}^* \mathrm{d}A(T_{\mathrm{v}} - T_{\mathrm{i}}) \tag{15}$$

$$c_v = \frac{N_{\mathrm{NH_3}} C_{p_{\mathrm{NH_3v}}} + N_{\mathrm{H_2O}} C_{p_{\mathrm{H_2Ov}}}}{h_v} \tag{16}$$

Bubble dynamics

Various correlations have been determined to find the bubble diameter. However the Bhavaraju's correlation [21] is the most widely used one. It was shown that the liquid above the orifice can be divided into two regions, I and II. Region I is characterized by large bubble sizes, lower hold-up, and non-uniform distribution of the bubbles across the bottom of the absorber. The bubble properties in this region are determined by the bubble formation process at the orifice. In region II, the bubble properties are determined by the bulk liquid motion. Bhavaraju *et al.* showed that the bubble break-up phenomenon occurs in region II and is related to liquid turbulence rather than the gas turbulence at the orifice.

Based on the gas flow rate, the bubble formation is divided into three regimes with very low gas rates, moderately high gas flow rates and very high gas rates. The expressions for the bubble diameter in these regions are tabulated in tab. 4.

The orifice number and the orifice diameter are adjusted using eq. (17):

$$V_V = \frac{m_{\mathrm{L(final)}} - m_{\mathrm{L(initial)}}}{\rho_{\mathrm{v}} A_0 n_0} = \frac{m_{\mathrm{abs}}}{\rho_{\mathrm{v}} A_0 n_0} \tag{17}$$

The absolute vapor velocity [21] is determined using eqs.(18) and (19):

$$V_{\mathrm{V}} = \frac{\mathrm{g}\rho_{\mathrm{L}}}{18\mu_{\mathrm{L}}}\left[\frac{6\sigma d_0}{\mathrm{g}(\rho_{\mathrm{L}} - \rho_{\mathrm{g}})}\right]^{2/3} \quad \text{for} \quad \mathrm{Re_B} < 1 \tag{18}$$

Table 4. Bhavaraju's correlations for bubble diameter

Very low gas rates	$Q_{V/O} \prec Q_t = \frac{\pi g \Delta\rho}{108\mu_L}\left[\frac{6\sigma d_0}{g(\rho_L-\rho_g)}\right]^{4/3}$ for $Re_B \le 1$ $Q_{V/O} \prec Q_t = 0.32 g^{0.5}\left[\frac{6\sigma d_0}{g(\rho_L-\rho_g)}\right]^{4/3}$ for $Re_B \gg 1$	$d_B = \left[\frac{6\sigma d_0}{g(\rho_L-\rho_g)}\right]^{1/3}$ $Re_B = \frac{\rho_L V_v d_B}{\mu_L}$
Moderately high gas rates	$Q_{V/O} \succ Q_t$ and $Re_{ol} < 2000$ $Re_{ol} = \frac{4\rho_L Q_{V/O}}{\pi d_0 \mu_L}$	$\frac{d_B}{d_0} = 3.23(Re_{ol})^{-0.1}(Fr_0)^{0.21}$ $Fr_0 = \frac{Q_{V/O}}{g d_0^5}$
Very high gas rates	$Re_{ol} > 2000$ (a) For $d_b < d_{bm}$ (b) d_{BE} =0.0045 m < $d_{bm} < d_b$ (c) For d_{BE} (=0.0045 m) < d_{bm}	(a) $\frac{d_B}{d_0} = 3.23(Re_{ol})^{-0.1}(Fr_0)^{0.21}$ (b) $d_{bm} = 0.7\left[\frac{\sigma^{0.6}}{\rho_L^{0.2}\left(\frac{P}{V}\right)^{0.4}}\right]\left(\frac{\mu_{app}}{\mu_G}\right)^{0.1}$ d_b = smallest (d_b, d_{bm}) (c) d_{BE} = 0.0045 m

$$V_V = \left(\left\{\frac{2\sigma}{\rho_L}\left[\frac{g(\rho_L-\rho_g)}{6\sigma d_0}\right]^{1/3}\right\} + \left\{\frac{g}{2}\left[\frac{6\sigma d_0}{g(\rho_L-\rho_g)}\right]^{1/3}\right\}\right)^{1/2} \quad \text{for} \quad Re_B \gg 1 \tag{19}$$

After determining the vapor velocity, the eqsuations in tab. 4 are used to determine the bubble diameter.

Interfacial area and gas hold-up

The liquid vapor interfacial area and gas hold-up play an important role in the mass transfer operation which determines the absorption rate. The interfacial area affects the volumetric mass transfer coefficient and the gas hold-up, ε_v influences the interfacial area [22]. The interfacial area is also influenced by the mean bubble diameter, d_B represented by eq. (26). This correlation for the mean bubble diameter was given by Akita and Yoshida [17] and Hikita *et al.* [23]. Gas hold-up depends on the superficial vapor velocity and the various properties of the weak solution and the vapor. It was found that gas hold-up in aqueous electrolyte solutions is slightly larger than in pure liquids or non-electrolyte solutions. Hence a correction factor *f* is used in the case of electrolyte solutions. In order to calculate the gas hold-up, many correlations have been determined. However for the current application, the gas hold-up is calculated using the correlation given by Deckwer and Schumpe [24]. This correlation is shown in eqs. (20) and (21):

$$\varepsilon_V = \frac{V_V}{V_{sb}} \quad \text{if} \quad V_V \le V_{trans} \tag{20}$$

$$\varepsilon_V = \frac{V_{trans}}{V_{sb}} + \frac{V_V - V_{trans}}{V_{lb}} \quad \text{if} \quad V_V \succ V_{trans} \tag{21}$$

$$V_{sb} = \frac{2.25\sigma}{\mu_L}\left(\frac{\rho_L \sigma^3}{g\mu_L^4}\right)^{-0.273}\left(\frac{\rho_L}{\rho_V}\right)^{0.03} \tag{22}$$

$$V_{bl} = \frac{\sigma}{\mu_L}\left(\frac{V_{sb}\mu_L}{\sigma} + \left\{2.4\left[\frac{\mu_L(V_V - V_{trans})}{\sigma}\right]^{0.757}\left(\frac{\rho_L\sigma^3}{g\mu_L^4}\right)^{-0.077}\left(\frac{\rho_L}{\rho_V}\right)^{0.077}\right\}\right) \tag{23}$$

$$\frac{V_{trans}}{V_{sb}} = 0.5\exp\left(-193\rho_V^{-0.61}\mu_L^{0.5}\sigma^{0.11}\right) \tag{24}$$

The interfacial area for a spherical bubble is given by the eq. (25) [17]:

$$A_i = 6\frac{\varepsilon_v}{d_B} \tag{25}$$

where

$$d_B = 26D_c\left(\frac{g\rho_L D_c^2}{\sigma}\right)^{-0.5}\left(\frac{g\rho_L^2 D_c^3}{\mu_L^2}\right)^{-0.12}\left[\frac{V_V}{(gD_c)^{0.5}}\right]^{-0.12} \tag{26}$$

However, if $\varepsilon_v < 0.14$, Akida and Yoshida [17] presented the expression shown in eq. (27) to estimate the interfacial area:

$$A_i = \frac{\varepsilon_V^{1.13}}{3D_c}\left(\frac{g\rho_L D_c^2}{\sigma}\right)^{0.5}\left(\frac{g\rho_L^2 D_c^3}{\mu_L^2}\right)^{0.1} \tag{27}$$

Mathematical model using control volume analysis

The control volume analysis involves solving the combined heat and mass transfer process in the system. The flow of the weak liquid solution and the vapor bubbles in the absorber has been mathematically modeled using a control volume analysis, fig. 2.

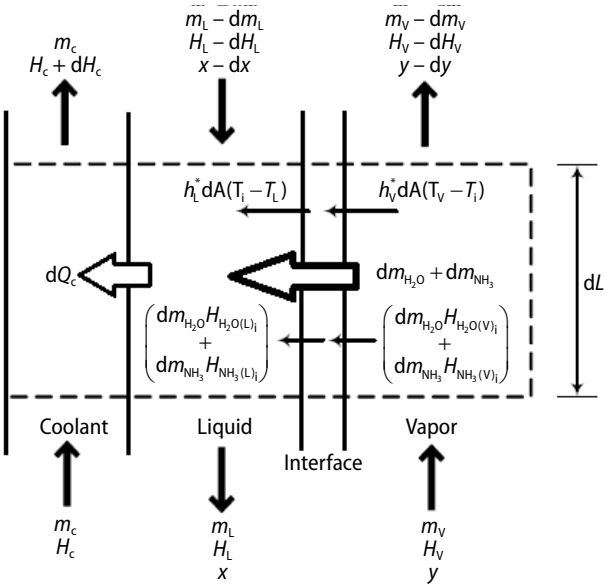

Figure 2. Schematic of the differential control volume of the absorber

The mass and concentration balance of each phase are given by the following equations.

– Mass balance for the liquid phase in the control volume:

$$m_L = (m_L - dm_L) + \\ +(N_{NH_3} + N_{H_2O})dA \tag{28}$$

– mass balance for the vapor phase in the control volume:

$$m_v = (m_v - dm_v) - \\ -(N_{NH_3} + N_{H_2O})dA \tag{29}$$

where dA is the mass transfer area between the liquid and the vapor phase.

– Concentration balance for the liquid phase in the control volume:

$$m_L x_L = (m_L - dm_L)(x_L - dx_L) + z(N_{NH_3} + N_{H_2O})dA \quad (30)$$

– Concentration balance for the vapor phase in the control volume:

$$m_v x_v = (m_v - dm_v)(x_v - dx_v) - z(N_{NH_3} + N_{H_2O})dA \quad (31)$$

– The energy balance equations for the control volumes of liquid and vapor phases are given:

$$m_L H_L + dQ_c = (m_L - dm_L)(H_L - dH_L) + h_L^* dA(T_i - T_L) + dm_{H_2O} H_{H_2O(L)_i} + dm_{NH_3} H_{NH_3(L)_i} \quad (32)$$

$$m_v H_v = (m_v - dm_v)(H_v - dH_v) + h_v^* dA(T_v - T_i) - dm_{NH_3} H_{NH_3(v)_i} - dm_{H_2O} H_{H_2O(v)_i} \quad (33)$$

The liquid-vapor interface is assumed to be at thermodynamic equilibrium. Mass fraction of weak solution and ammonia in the vapor at the interface can then be expressed:

$$x_{Li} = f(T_i, P) \quad (34)$$

$$x_{vi} = f(T_i, P) \quad (35)$$

Energy balance at the liquid-vapor interface gives:

$$h_L^* dA(T_i - T_L) + dm_{H_2O} H_{H_2O(L)_i} + dm_{NH_3} H_{NH_3(L)_i} = \\ = h_v^* dA(T_v - T_i) + dm_{H_2O} H_{H_2O(v)_i} + dm_{NH_3} H_{NH_3(v)_i} \quad (36)$$

The heat is transferred to the coolant through the liquid phase. The heat absorbed by the coolant can be found by an energy balance over the coolant-liquid interface, coolant, and global control volumes:

$$dQ_c = U dA(T_L - T_c) \quad (37)$$

$$dQ_c = m_c dH_c \quad (38)$$

$$dQ_c = \left[(m_L - dm_L)(H_L - dH_L) + (m_v - dm_v)(H_v - dH_v)\right] - (m_L H_L + m_v H_v) \quad (39)$$

where the overall heat transfer coefficient U combines the various thermal resistances in the path of the heat flow between the weak solution and coolant, and can be given:

$$\frac{1}{U} = \frac{1}{h_c} + R_{wall} + \frac{1}{h_{film}} \quad (40)$$

The coolant-side heat transfer coefficient h_c is based on the developing laminar flow conditions in the coolant tube [25]:

$$h_c = 0.026\left(\frac{kc}{t}\right) \mathrm{Re}_{plate}^{0.82} \mathrm{Pr}_c^{0.32} \quad (41)$$

where Re_{plate} is the Reynolds number for flow in the cooling plate and Pr_c is the Prandtl number of the coolant.

Numerical technique

A finite difference numerical method is used to solve the system of non-linear ordinary differential equations. The model is subjected to the given inlet conditions of the liquid, vapor

and coolant flow regimes. The absorber is divided into differential elements and the analysis is carried over the individual elements. An element of length ΔL is considered. The convergence criterion assumed is 10^{-5}.

If the weak ammonia-water liquid solution and ammonia vapor conditions were known at the bottom section of any incremental element, then the conditions of weak ammonia-water liquid solution and of the ammonia vapor at the top section would be obtained. Calculation of the unknown conditions requires the determination of the heat and mass transferred between the weak ammonia-water liquid solution and the ammonia vapor phases, which are obtained using eqs. (1)-(41). As given by eq. (1), mass transfer depends on the value of the interface mass fraction x_{Li} and x_{vi} and the ratio z, which are obtained from the interface temperature. On the other hand, the heat transfer given by eqs. (13) and (15) depends on the interface temperature T_{i} and the ammonia and total mass transferred. For this reason, a trial and error procedure must be implemented to solve these equations, fig. 3.

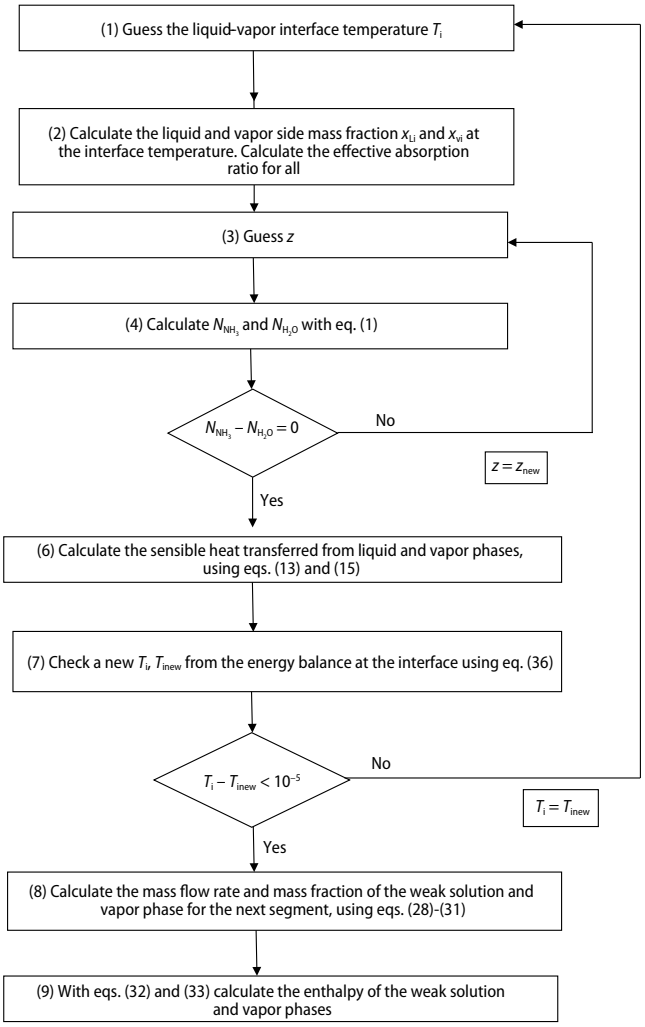

Figure 3. Calculation procedure

Algorithm presented at fig. 3, uses two iterative loops to obtain the values of the concentration ratio z and the interface temperature. Once these parameters are calculated, the weak ammonia-water liquid solution and the ammonia vapor conditions at the top section of any incremental element are computed. Thus, the input parameters for solving the next section are known. The heat and mass transfer coefficients and the transfer area are obtained from the input conditions and assumed constant throughout the incremental element.

Results and discussion

The data required by the computer code are the absorber geometry and material thermal properties, as well as the absorber operating conditions. The results obtained by matlab code are the variation of several parameters such as: the effective absorption rate, the solution concentration, the vapor concentration, the bubble diameter and the gas hold-up on the absorber performance.

Figure 4 depicts the variation of the effective absorption ratio for two different types of

nanoparticles as Cu and Al_2O_3 with the concentration of nanoparticles. It is clearly implied that the addition of Cu nanoparticles is the most effective absorption ratio compared to the Al_2O_3 nanoparticles. The enhancement was found to be higher for nanofluids made from Cu.

Figure 5 shows the profiles of solution concentrations in the case without any addition, in the case of the binary nanofluids (NH_3/H_2O binary mixture with Cu nanoparticles) and in the case of (NH_3/H_2O binary mixture with CuO nanoparticles) when the mass fraction of nanoparticles is 0.1%. It is shown that, the enhancement of the absorber performance was found to be higher for the binary nanofluids (NH_3/H_2O binary mixture with Cu nanoparticles) compared to that (NH_3/H_2O binary mixture with CuO nanoparticles) and to that any addition. The nanofluids made from Cu exhibited the highest increase in the enhancement of bubble absorption performance among the CuO nanoparticles.

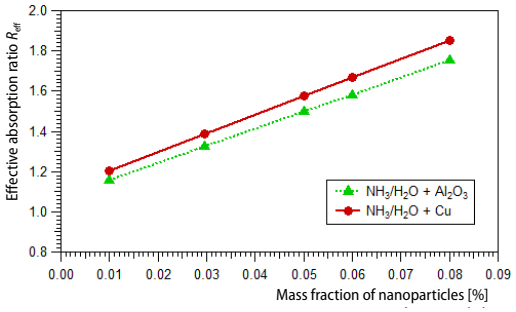

Figure 4. The effective absorption ratio for all binary nanofluids as a function of concentration of nanoparticles

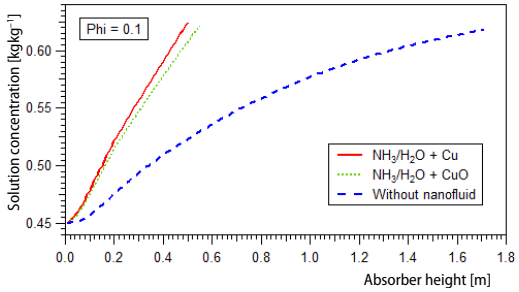

Figure 5. Variation of solution concentration along the absorber height for two type of binary nanofluid

The solution concentration profiles as a function of concentration of nanoparticles is illustrated in fig. 6. The concentration of nanoparticles range was selected as 0, 0.05, and 0.1%. The analysis showed that in the case without any addition the solution concentration increase gradually near the bottom of the absorber, while it increases dramatically through the whole vertical location in the case with addition of Cu nanoparticles. As expected, increasing the concentration of nanoparticles results in an increase in absorption rate. Note that absorption rate varies by changing physical proprieties of the mixture when adding nanoparticles. The absorber length required of complete absorption decrease as the concentration of nanoparticles increase.

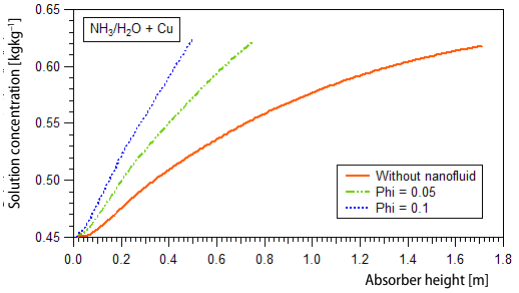

Figure 6. Variation of solution concentration along the absorber height for binary nanofluid with Cu

To find the effect of the concentration of nanoparticles on the absorber size we have shows in fig. 7 the vapor concentration as a function of concentration of nanoparticles. As evident from the plots, the required length decreases as the concentration of nanoparticles increases. It is found that the concentration of nanoparticles has a significant effect on the absorber size.

Figure 8 shows the bubble diameter during the bubble absorption process for without any addition and for the binary nanofluid (NH_3/H_2O binary mixture with Cu nanoparticles) when

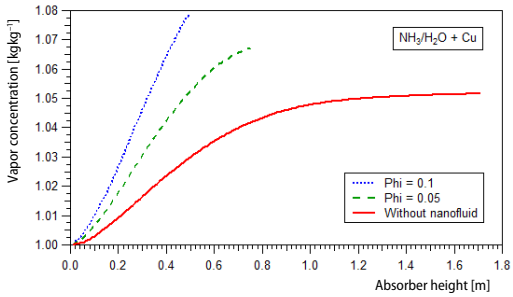

Figure 7. Variation of vapor concentration along the absorber height for binary nanofluid with Cu

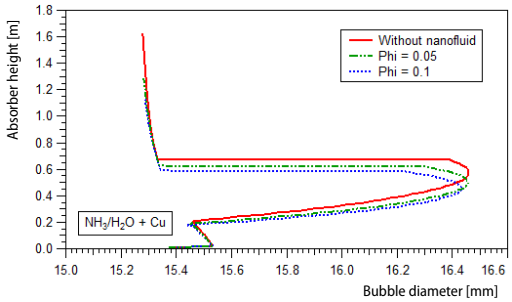

Figure 8. Variation of bubble diameter along the absorber height for binary nanofluid with Cu

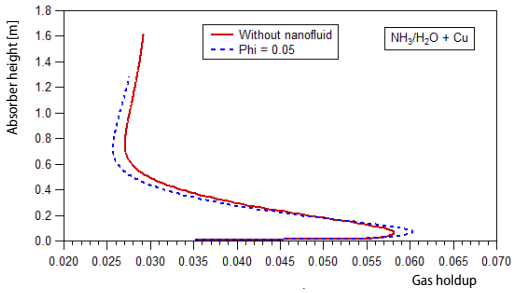

Figure 9. Variation of gas holdup along absorber height for binary nanofluid with Cu

the concentration of nanoparticles is 0.05% and 0.1%. In the case with the Cu 0.1% binary nanofluid, the bubble diameter $1.5214 \cdot 10^{-2}$ m while it rises up to $1.5225 \cdot 10^{-2}$ m in the case without the nanoparticles. The size of bubble can be successfully reduced by adding nanoparticles. The bubble size in the binary mixture without nanoparticles is larger than that in the binary nanofluid.

Figure 9 shows the variation of gas hold up along the absorber height for (NH_3/H_2O binary mixture with Cu nanoparticles) when the concentration of Cu nanoparticles is 0.05%. The addition of nanoparticles in the binary mixture resulted in an increase in gas hold up witch increase the absorption rate.

Conclusions

In the present study, the main objective is to investigate the heat and mass transfer enhancement by using binary nanofluids in NH_3/H_2O bubble absorption processes and to find the effect of some parameters such as the concentration of nanoparticles, kinds of additives of nanoparticles, the bubble diameter, and the gas holdup on the absorption rate. The analysis has been carried out developing a differential mathematical model based on mass and energy balances and the heat and mass transfer equations using matlab. The mass transfer enhancement and the highest effective absorption is much more significant in the case of the binary nanofluids with Cu nanoparticles.

Nomenclature

A – area, [m^2]
A_p – projected area, [m^2]
C_p – specific heat, [kJkg^{-1}K^{-1}]
D – diffusivity, [m^{2}s^{-1}]
d – diameter, [m]
dm – mass flux transferred, [kgs^{-1}]
Fr$_o$ – Froude's number, [–]
g – gravitational acceleration, [ms^{-2}]
H – enthalpy, [Jkg^{-1}]
h – heat transfer coefficient, [Wm^{-2}K–1]
K – overall mass transfer coefficient, [ms^{-1}]
k – thermal conductivity, [Wm^{-1}K^{-1}]
L – length of plate, [m]
M – molecular weight, [kgkmol^{-1}]
m – mass flow rate, [kgs^{-1}]
N – molar flux, [kmolem^{-2}s^{-1}]
Nu – Nusselt number, [–]
P – pressure, [Pa]
phi – concentration of nanoparticle, [%]
Pr – Prandtl number, [–]
Q – heat transfer rate, [kW]
Re – Reynold's number, [–]

R_{eff} – effective absorption ratio, [–]
R_{wall} – conduction resistance, [m^2KkW^{-1}]
Sc – Schimdt's number, [–]
Sh – Sherwood number, [–]
St – Stanton number, [–]
T – temperature, [K]
t – thickness of the cooling plate, [m]
U – overall heat transfer coefficient, [$kWm^{-2}K^{-1}$]
W – absorber width, [m]
x – mass concentration, [$kgkg^{-1}$]
z – ratio of ammonia mass flow rate to the total mass flow rate, [–]

Greek symbols

β – diffusivity, [m^2s^{-1}]
μ – dynamic viscosity, [$kgm^{-1}s^{-1}$]
ρ – density, [kgm^{-3}]
σ – surface tension, [Nm^{-1}]

Subscripts

abs – absorption process
b – bubble
bn – binary nanofluid
c – coolant
i – interface
L – liquid phase
NP – nanoparticle
o – orifice
Plate – plate
sen – sensible
v – vapor phase

References

[1] Ramanathan, A., Gunasekaran, P., Simulation of Absorption Refrigeration System for Automobile Application, *Thermal Science*, *12* (2008), 3, pp. 5-13
[2] Agboola, O., *et al.*, Thermo-Economic Performance of Inclined Solar Water Distillation Systems, *Thermal Science*, *19* (2015), Suppl. 2, pp. S557-S570
[3] Benhmidene, A., *et al*., Effect of Operating Conditions on the Performance of the Bubble Pump of Absorption-Diffusion Refrigeration Cycles, *Thermal Science*, *15* (2011), 3, pp. 793-806
[4] Luo, C., *et al.*, Heat Transfer Characteristics of Ammonia-Water Falling Film Generation Outside a Vertical Tube, *Thermal Science*, *21* (2017), 3, pp. 1251-1259
[5] Shim, S.-M., *et al.*, A Numerical Evaluation of Prediction Accuracy of CO_2 Absorber Model for Various Reaction Rate Coefficients, *Thermal Science*, *16* (2012), 3, pp. 877-888
[6] Ben Hamida, M. B., Charrada, K., Natural Convection Heat Transfer in an Enclosure Filled with an Ethylene Glycol-Copper Nanofluid under Magnetic Fields, *Numerical Heat Transfer, Part A: Applications: An International Journal of Computation and Methodology, 67* (2014), 8, pp. 902-920
[7] Kim, J. K., *et al*., Absorption Performance Enhancement by Nanoparticles and Chemical Surfactants in Binary Nanofluids, *International Journal of Refrigeration*, *30* (2007), 1, pp. 50-57
[8] Wu, W., *et al*., Enhancement on NH_3/H_2O Bubble Absorption in Binary Nanofluids by Mono Nano Ag, *J. Chem. Ind. Eng. Soc. China, 61* (2010), 5, pp. 1112-1117
[9] Pang, C., *et al*., Mass Transfer Enhancement by Binary Nanofluids (NH_3/H_2O + Ag Nanoparticles) for Bubble Absorption Process, *International Journal of Refrigeration*, *35* (2012), 8, pp. 2240-2247
[10] Ma, X., *et al*., Enhancement of Bubble Absorption Process Using a CNTs-Ammonia Binary Nanofluid, *International Communications in Heat and Mass Transfer*, *36* (2009), 7, pp. 657-660
[11] Kang, Y. T., *et al*., Heat and Mass Transfer Enhancement of Binary Nanofluids for H_2O/LiBr Falling Film Absorption Process, *International Journal of Refrigeration*, *31* (2008), 5, pp. 850-856
[12] Su, F., *et al*., A Numerical Model for Ammonia/Water Absorption from a Bubble Expanding at a Submerged Nozzle into a Binary Nanofluid, *Journal of Nanotechnology in Engineering and Medicine*, *5* (2014), 1, 011006
[13] Yang, L., *et al*., Experimental Study on Enhancement of Ammonia-Water Falling Film Absorption by Adding Nano-Particles, *International Journal of Refrigeration*, *34* (2011), 3, pp. 640-647
[14] Kim, J. K., *et al*., The Effect of Nanoparticles on the Bubble Absorption Performance in a Binary Nanofluid, *International Journal of Refrigeration*, *29* (2006), 1, pp. 22-29
[15] Kim, J. K., *et al*., The Effects of Nanoparticles on Absorption Heat and Mass Transfer Performance in NH_3/H_2O Binary Nanofluids, *International Journal of Refrigeration*, *33* (2010), 2, pp. 269-275
[16] Kim, H., *et al*., Heat and Mass Transfer Enhancement for Falling Film Absorption Process by SiO_2 Binary Nanofluids, *International Journal of Refrigeration*, *35* (2012), 3, pp. 645-651
[17] Akita, K, A., Yoshida, F., Bubble Size, Interfacial Area, and Liquid Mass Transfer Coefficient in Bubble Columns, *Industrial and Engineering Chemistry Process Design and Development*, *13* (1974), 1, pp. 84-91
[18] Clift, R., *et al*., *Bubbles, Drops and Particles*, Academic Press Inc., New York, USA, 1978

[19] Chilton, T. H., Colburn, A. P., Mass Transfer (Absorption) Coefficients Prediction from Data on Heat Transfer and Fluid Friction, *Ind. Engrg. Chem., 26* (1934), 11, pp. 1183-1187
[20] Treybal, R. E., *Mass Transfer Operations*, McGraw Hill Publications, New York, USA, 1955
[21] Bhavaraju, S. M., *et al*., The Design of Gas Sparged Devices for Viscous Liquid Systems, *AIChE Journal, 24* (1978), 3, pp. 454-466
[22] Kang, Y. T., *et al.*, Ammonia Water Bubble Absorber with a Plate Heat Exchanger, *ASHRAE Transactions*, *104* (1998), 1, pp. 1565-1575
[23] Hikita, H., *et al*., The Volumetric Liquid-Phase Mass Transfer Coefficient in Bubble Columns, *The Chemical Engineering Journal*, *22* (1981), 1, pp. 61-69
[24] Deckwer, W.-D., Schumpe, A., Improved Tools for Bubble Column Reactor Design and Scale-up, *Chemical Engineering Science*, *48* (1993), 5, pp. 889-911
[25] Azbel, D., *Fundamentals of Heat Transfer for Process Engineering*, Noyes Publications, Park Ridge, N. J., USA, 1984

Paper submitted: March 13, 2017
Paper revised: July 30, 2017
Paper accepted: July 30, 2017